Assessing Zethrene Derivatives as Singlet Fission Candidates Based on Multiple Descriptors

Xingyu Liu,[†] Rithwik Tom,[‡] Siyu Gao,[†] and Noa Marom*,[†],[‡],¶

†Department of Materials Science and Engineering, Carnegie Mellon University, Pittsburgh, PA, 15213

‡Department of Physics, Carnegie Mellon University, Pittsburgh, PA, 15213

¶Department of Chemistry, Carnegie Mellon University, Pittsburgh, PA, 15213

E-mail: nmarom@andrew.cmu.edu

Abstract

Singlet fission (SF) is a process where one singlet exciton splits into two triplet excitons. Utilizing SF may potentially increase the efficiency of solar cells beyond the Shockley-Queisser limit. In order to discover new SF materials, predictive descriptors for SF performance are needed. We consider multiple descriptors in order to assess several zethrene derivatives as candidate materials for intermolecular SF in the solid state. The descriptors include single molecule multi-radical characters, many-body perturbation theory calculations of the thermodynamic driving force for SF and the singlet exciton charge transfer character in crystals, and a kinetic model based on molecular dimers extracted from the crystal structures. The zethrenes are compared to acenes known to exhibit SF with respect to these descriptors. The results indicate that all zethrene and heptazethrene derivatives studied here may exhibit SF. In particular,

7,14-bis(2,4,6-trimethylphenyl)dibenzo[de,mn]naphthacene (Z-T) emerges as a promising candidate. Its SF driving force is higher than tetracene, whose fission process is slightly endoergic, but lower than pentacene; Its singlet exciton charge transfer character is close to pentacene; and its crystal packing leads to a higher SF rate than other zethrene derivatives. Therefore, it may undergo fast SF with high energy efficiency. The approach of considering multiple descriptors may be useful for evaluating additional candidate materials for SF.

Introduction

Singlet fission (SF) is a spin-allowed conversion process in organic chromophores, where one singlet-state exciton (S_1) splits into two triplet-state excitons (T_1). SF is considered as a possible path to surpass the Shockley-Queisser limit of solar cell efficiency, which is around 30%, depending on the absorber's band gap. The Shockley-Queisser limit is based on the assumption that one exciton is generated per absorbed photon. SF may increase power conversion efficiency by reducing the energy loss caused by the thermalization of high-energy photons. Rather than losing the excess energy to heat, high-energy photons may undergo SF and produce two charge carriers per photon. Theoretical analysis has suggested that efficiency as high as 47% may be achieved in a two-gap tandem photovoltaic device, based on SF. 9

The realization of commercial SF-based solar cells is hindered by the dearth of suitable materials. ¹⁰ To be viable for commercial applications, in addition to having good SF performance, a material should be relatively straightforward to synthesize and should have a sufficiently long service life under working conditions, including exposure to sunlight and ambient environment. Crystalline oligoacenes have demonstrated exceptional quantum yield and fission rates. ^{11–13} However, insufficient photo-stability and poor solubility of large acene molecules preclude their usability as absorbers in photovoltaic devices. Some stabilized acene derivatives have been predicted to be potential SF materials, ^{14,15} with ex-

perimental verification still pending. Among the emerging classes of SF materials are 1,3-diphenylisobenzofuran¹⁶ and rylene derivatives.^{17–21} However, they have yet to be incorporated into a functioning solar cell.

The search for new SF materials requires predictive descriptors for the performance of a candidate material. SF may be intramolecular ^{22–24} or intermolecular. ^{25,26} Most of the SF-based solar cells developed to date have relied on intermolecular SF in the solid state. ^{27–30} The efficiency of intermolecular SF depends on both the molecular properties and the crystal packing. ^{31–35} In fact, different polymorphs may have a significantly different performance. ^{16,36,37} Therefore, it is important to consider both single molecule and crystal descriptors.

The primary criterion for a material to undergo SF is that the energy difference between S_1 and $2T_1$ should be greater than 0 eV, in order to provide the thermodynamic driving force for the process:

$$E_{S_1} - 2E_{T_1} \ge 0 \tag{1}$$

In addition to the energetic requirements, descriptors related to the nature of excitons in molecular crystals may correlate with SF performance. There is a growing body of experimental evidence indicating that an intermediate charge transfer state may be involved in SF, ^{3,38-41} although in some experiments an intermediate state was not observed. ⁴² Therefore, exciton character has been considered as a secondary descriptor associated with efficient inter-molecular SF in the solid state. ^{15,21,36,43} A singlet exciton with a degree of charge transfer character (%CT), meaning that the hole and the electron are not located on the same molecule, is thought to be beneficial to SF. ^{3,25,44} Another facet of exciton behavior is diffusion. Chan et al. ²⁶ have suggested that diffusion of the singlet exciton in a tetracene crystal provides entropic driving force for SF, which may compensate for enthalpic loss and lead to high quantum yield. They estimated the entropic driving force for SF in crystalline tetracene based on experimentally measured values of the exciton diffusion length. Kolomeisky et al. ⁴⁵ have used similar considerations of exciton delocalization to estimate the entropic contribution in tetracene, pentacene, and hexacene by counting neighbouring chromophores from

delocalized singlet excitons and ways in which multiexcitons can separate within the Dexter radius. However, their model only applies to acenes with a herringbone crystal packing, in which excitons are delocalized over a layer of molecules. ^{21,46} Currently, there is no model of the entropic contribution to SF, which does not rely on information from experiments and is generally applicable across different classes of materials.

It has been suggested that compounds with biradicaloid character could be promising SF chromophores. ⁴⁷ In order to quantify this, Nakano et al. ^{20,48,49} have proposed a descriptor based on multi-radical characters as an indicator of the SF potential for molecules. The diradical character, y_0 , and the tetraradical character, y_1 , are calculated based on the occupation numbers of the highest occupied and lowest unoccupied natural orbitals (HONO/LUNO), and on the occupation numbers of the HONO-1 and LUNO+1, respectively. The values of y_i range from 0 to 1. They reflect the degree of open shell character of the molecular ground state. (y_0, y_1) values of (0, 0), (1, 0), and (1, 1) represent a closed-shell ground state, a pure diradical, and a pure tetraradical, respectively. Based on a linear H_4 model, it has been proposed that the energetic criterion for SF is satisfied when y_0 of a molecule is larger than 0.1 except for highly tetraradical cases. ⁴⁸ It has been shown that molecules with intermediate y_0 paired with small y_1 would satisfy the SF feasibility condition. Several known SF chromophores have been evaluated and new candidates have been proposed based on this descriptor. ^{20,50-53} Here, we examine whether this descriptor correlates with the results of many-body perturbation theory for the SF driving force of chromophores.

In addition to thermodynamic considerations, kinetics affect SF performance. A number of recent papers have studied the effect of crystal packing and exciton delocalization on SF kinetics. ^{45,54–56} Yost et al. ⁵⁶ have used the Bixon-Jortner (BJ) ⁵⁷ rate expression for estimating SF rates in molecular crystals. The electronic coupling and driving force were assumed to be the only material dependent parameters in the rate expression. The electronic coupling of all possible molecule pairs were computed using Configuration interaction based on constrained density functional theory. ⁵⁸ Quantum mechanics/ molecular mechanics (QM/MM)

techniques were used to model the electronic states of a dimer embedded in the electrostatic crystal field. A few parameters of the BJ model were obtained from experimental data for aceneoid systems. The driving force was chosen according to the backbone of the material. With these assumptions, reasonable agreement was obtained with experimental SF rates for a class of tetracene and pentacene derivatives. Kolomeisky et al. 45 have used a three-state model (initial singlet, multiexciton, separated triplet) for singlet fission dynamics to obtain order of magnitude estimates of SF rate. Rate calculations were based on the Fermi Golden rule and first passage time model 59 with some parameters obtained from experiments. Using this model, they have explained the experimentally observed magnitude difference between the SF rates in tetracene and pentacene.

Michl et al. 32 have proposed a model for comparing the SF rates among molecular dimers with different geometries, implemented in the Simple code package. This model could offer insight into how to manipulate the packing of molecules in a crystal to achieve the optimal SF performance by finding the molecular pair geometries that maximize the SF rate. The model does not rely on experimental information and may be applied to any material. However, it cannot be applied for comparisons between materials. Under the assumption that the thermodynamic conditions for SF are already met, the model focuses on the rate of formation of the singlet biexciton state from the initial singlet state. The biexciton state is the complex of two molecules in the triplet state, which subsequently separates into two independent triplet excitons. Marcus theory is used to calculate the rate of biexciton formation in molecular dimers. The renormalization energy for the Marcus rate is assumed to be independent of the molecular pair geometry. The SF rate is calculated based on the Fermi golden rule with the matrix elements calculated using a frontier orbital model, which contains only the highest occupied molecular orbital (HOMO) and lowest unoccupied molecular orbital (LUMO) of the two molecules. The singlet configuration is represented by $^{1}(hA \rightarrow lA)$ and $^{1}(hB \rightarrow lB)$, where hA, lA, hB, lB correspond to HOMO and LUMO of molecules A and B, respectively. Fission is mediated by charge transfer states, in which an electron is transferred

from one molecule to the other. The final biexciton state is represented by two lowest triplet states, ${}^3(hA \to lA)$ and ${}^3(hB \to lB)$ coupling into an overall singlet state. Simple calculates only superexchange electronic couplings involving CT states. Because Simple is designed to identify optimal dimer geometries for singlet fission, the contribution from the direct term is neglected. 60 The contribution from superexchange coupling has been found to be more prominent than direct coupling in several cases with high SF rates. ${}^{61-63}$ Others have also considered the direct term. 53 The model is further simplified by neglecting intermolecular overlap of orbitals and assuming zero differential overlap. These approximations were built into Simple for fast evaluation and are strictly valid only near local maxima. The frontier orbitals are expanded in a natural atomic orbital (NAO) basis. The main limitations of Simple are that many-body interactions, and the possibility that the initial singlet exciton is delocalized on more than two molecules in a crystal are neglected. Moreover, Simple does not take into account other processes that can compete with SF. Here, we apply the Simple model to molecular dimers extracted from crystal structures to assess the effect of crystal packing on of SF rates.

$$\mathbf{Z}-\mathbf{P}\colon \mathbf{A}=-\mathbf{H}$$

$$\mathbf{Z}-\mathbf{D}\colon \mathbf{A}=-\mathbf{H}$$

$$\mathbf{Z}-\mathbf{T}\colon \mathbf{A}=-\mathbf{H}$$

$$\mathbf{Z}-\mathbf{T}\colon \mathbf{A}=-\mathbf{H}$$

$$\mathbf{Z}-\mathbf{T}\colon \mathbf{A}=-\mathbf{H}$$

$$\mathbf{Z}-\mathbf{T}\colon \mathbf{A}=-\mathbf{H}$$

Figure 1: Molecular structures of zethrene and its derivatives Z-P, Z-D, Z-T, and Z-B, and heptazethrene derivative HZ-BTB. The abbreviated names are listed beside the corresponding molecules.

Zethrenes have been drawing increasing attention as potential high-efficiency SF chro-

mophores.⁶⁴ However, due to their unstable nature, zethrenes have not been incorporated into a functioning solar cell device. Functionalization with side groups has been explored as a strategy for stabilizing zethrenes.^{65,66} The effect of backbone length and side group functionalization on the crystal structure and excitonic properties of zethrene derivatives has not been well studied. A systematic investigation could provide guidance for designing zethrene derivatives as feasible SF materials.

Here, we examine a series of zethrene derivatives, whose molecular structures are shown in Figure 1. These include the zethrene derivatives dibenzo [de, mn] naphthacene (Z-P), 7,14diphenyldibenzo [de, mn] naphthacene (Z-D), 7,14-bis (2,4,6-trimethylphenyl) dibenzo [de, mn] naphthacene (Z-T), and 7,14-Di-n-butyldibenzo [de,mn] naphthacene (Z-B), and the heptazethrene derivative 7,15-bis(4-t-butylphenyl)-1,9-dimethylheptazethrene (HZ-BTB). The corresponding Cambridge Structural Database (CSD) reference codes are KAGGEG, 67 KAGFOP, 68 KAGGAC, 68 KAGGIK, 68 and OBOHUL. 69 The excited-state properties of the zethrene derivatives are calculated using many-body perturbation theory (MBPT) methods, based on the GW approximation and the Bethe Salpeter equation (BSE). To explore the correlations between the multi-radical characters and the exciton energies among this class of zethrenes, we calculated the diradical character y_0 and tetraradical character y_1 . To elucidate the effect of crystal packing, we use Simple to find the relative SF rates of different dimers in crystals of zethrene derivatives that share the same backbone. We find that Z-T could be an outstanding SF candidate given its favorable thermodynamic driving force, decent exciton charge transfer character, and outstanding fission rates compared to other zethrene derivatives. Z-P could exhibit comparable singlet fission performance to the pentacene derivative diphenylpentacen (DPP). Based on the Simple analysis of Z-T, Z-D, and Z-B, the fission rate in zethrene derivatives may be modified by introducing side groups that alter the crystal packing. Relatively small geometrical differences between molecular dimers in different crystal structures may lead to significant differences in the fission rate. HZ-BTB satisfies both the energetic conservation criterion and suitable exciton behavior, which makes it possible SF candidate. However, the worst energy efficiency is identified in HZ-BTB among the zethrene series. Thus, HZ-BTB might not be a practical SF candidate to advance the power conversion efficiency of solar cells.

Methods

Starting geometries were extracted from the Cambridge Structural Database (CSD). Geometry relaxations of the isolated molecules and the crystal structures was performed using the FHI-aims⁷⁰ electronic structure package. Density functional theory (DFT) was employed with the generalized gradient approximation of Perdew, Burke and Ernzerhof (PBE)⁷¹ functional coupled to the Tkatchenko-Scheffler (TS) pairwise dispersion method.⁷²

Many-body perturbation theory calculations within the GW approximation and the Bethe-Salpeter equation (BSE)^{73–75} were performed to investigate the excitonic properties for both gas-phase and solid-state zethrenes and heptazethrene. Single molecule calculations were performed using FHI-aims,^{76,77} using PBE as the mean-field starting point and the aug2tier2 basis sets. The PBE functional yields a closed shell ground state for all zethrene and heptazethrene derivatives studied here, which is consistent with experimental observations.⁶⁶ The subsequent BSE calculation within the Tamm–Dancoff approximation (TDA)⁷⁸ was performed using 30 unoccupied and 30 occupied states.

GW+BSE calculations for molecular crystals were performed using the BerkeleyGW code.⁷⁹ Quantum ESPRESSO⁸⁰ was used to compute the mean-field eigenvectors and eigenvalues and to generate the mean-field coarse-grid and fine-grid wave functions with the PBE exchange-correlation functional. Troullier-Martins norm-conserving pseudopotentials⁸¹ were used and the kinetic energy cutoff was set to 50 Ry. About 550 unoccupied bands were included in the GW calculation. The static remainder correction was applied to accelerate the convergence with respect to the number of unoccupied states.⁸² 24 valence bands and 24 conduction bands were included in the BSE calculation within the TDA. The exciton wave

functions were converged based on the threshold proposed in Ref. 15

We note that the PBE exchange-correlation functional was selected as the starting point for GW+BSE calculations thanks to its computational efficiency. Although using more computationally expensive hybrid functionals as a starting point for GW+BSE calculations may improve the accuracy, PBE has been found to be an adequate starting point for polycyclic aromatic hydrocarbons (PAHs) because it produces qualitatively correct spectra. 36,83 The TDA has been found to improve the accuracy of triplet excitation energies obtained from GW+BSE calculations, while its effects on the accuracy of singlet excitation energies is still debated. 78,84 GW+BSE@PBE systematically underestimates the value of $E_{S_1}-2E_{T_1}$. 14,36,78,85 Therefore, we restrict the discussion to qualitative comparisons between the relative SF driving force of different materials, rather than absolute values of $E_{S_1}-2E_{T_1}$.

The diradical and tetraradical characters of the zethrene derivatives studied here were calculated following the procedure of Refs. 48,49 Multiple diradical characters were calculated based on the spin-projected unrestricted Hartree-Fock (PUHF) method, using the GAMESS package, 86 with 6-31G* basis sets. 87 The multi-radical characters, y_i , are calculated based on the occupation numbers of the HONO-i and LUNO+i. y_i is defined as:

$$y_i = 1 - \frac{2T_i}{1 + T_i^2} \tag{2}$$

where T_i is defined with n_{index} with its subscript indicating the index of the natural orbital:

$$T_i = \frac{n_{\text{HONO-}i} - n_{\text{LUNO+}i}}{2} \tag{3}$$

To calculate SF rates with the Simple code,³² dimers were extracted from the crystal structures of the zethrene derivatives Z-T, Z-D, and Z-B. Because Simple can only be used to compare SF rates between dimers of the same molecules, the side groups of Z-B, Z-D, and Z-T were removed and replaced by hydrogen atoms, whose positions were relaxed. For the same reason, Z-P, which has a planar backbone unlike the others, was not considered.

Dimers comprising molecules with a center of mass distance of 8 Å at most were considered. The frontier orbitals needed for Simple were calculated with the Gaussian 16 package ⁸⁸ using the restricted Hartree-Fock (RHF) method with the 6-311G basis set. Natural bond orbital (NBO) analysis version 3.1 was used within Gaussian for generating the natural atomic orbitals (NAO) for Simple. To evaluate the relative SF rates between dimers, the energy of CT states was set to 2 eV. The superexchange coupling values obtained for different dimers are provided in the SI.

The reorganization energy for Marcus theory, λ , was calculated based on the difference between the triplet excitation energies in the initial state geometry (with one molecule in the singlet excited state geometry and the other in the ground state geometry) and in the final state geometry (with both molecules in the triplet excited state geometry), $E[T_1, q(S_1)] + E[T_1, q(S_0)] - 2 \times E[T_1, q(T_1)]$ where q(X) stands for equilibrium geometry in the state X. Geometry optimizations in the excited states were performed with the Gaussian⁸⁸ code, using the B3LYP^{89,90} functional and 6-311G basis sets. The reorganization energy of the zethrene molecule studied here was found to be $\lambda = 0.77$ eV.

Results and discussion

We begin by evaluating the zethrene derivatives as isolated molecules. Figure 2 shows the tetraradical character, y_1 , as a function of the diradical character, y_0 . The known SF chromophores tetracene, pentacene, and two phenylated acene derivatives DPT and DPP are shown for comparison. Tabulated y_0 and y_1 values are provided in the Supporting Information (SI). Among the zethrene derivatives, both y_0 and y_1 increase with the zethrene backbone size from the zethrene derivatives to heptazethrene, which indicates a stronger open-shell character for larger zethrenes. Different side groups modify the multi-radical characters. Among the acenes, the phenyl side groups do not significantly change the multi-radical characters for DPT and DPP compared to tetracene and pentacene, respectively.

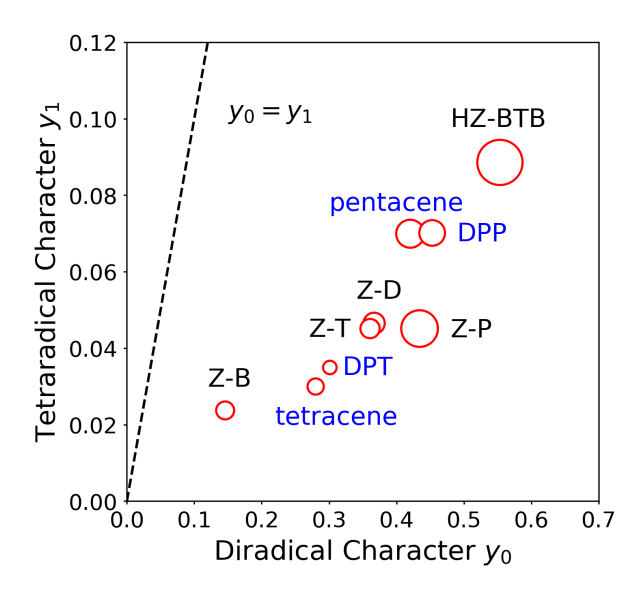


Figure 2: The tetraradical character, y_1 , as a function of the diradical character, y_0 . The radii of the red circles are proportional to the relative SF driving force $(E_{S_1}-2E_{T_1})$ calculated using GW+BSE@PBE. Zethrenes and acenes are labeled in black and blue, respectively.

The zethrene derivatives Z-T and Z-D have a slightly larger y_0 than tetracene and DPT, but smaller y_0 than pentacene and DPP. All zethrene and acene derivatives studied here are within the feasibility region for SF as defined by Minami et al. ⁴⁸ with moderate y_0 values between 0.1-0.6 and relatively low y_1 values, below 0.1. The radii of the red circles in Figure 2 are proportional to the relative SF driving force $(E_{S_1} - 2E_{T_1})$, calculated using GW+BSE@PBE. Tabulated values of excitonic properties are provided in the SI. In agreement with Refs., ^{48,51,53} chromophores with moderate y_0 paired with small y_1 have a favorable SF driving force. The highest molecular SF driving force is found for the heptazethrene derivative HZ-BTB, followed by the zethrene Z-P. The zethrene derivatives Z-B, Z-T, and Z-D, with smaller y_0 , have a smaller SF driving force than Z-P, HZ-BTB, pentacene, and DPP, but somewhat higher than tetracene and DPT. This means that within the SF feasibility range smaller y_0 is correlated with higher SF efficiency, in the sense that the energy loss is smaller. Our findings that zethrene derivatives with larger backbones yield higher y_0 and y_1 , as well as a higher SF driving force are in agreement with Naskar $et \ al.$ ⁹¹

Figure 3 shows the quasi-particle band structures of the crystalline zethrene derivatives,

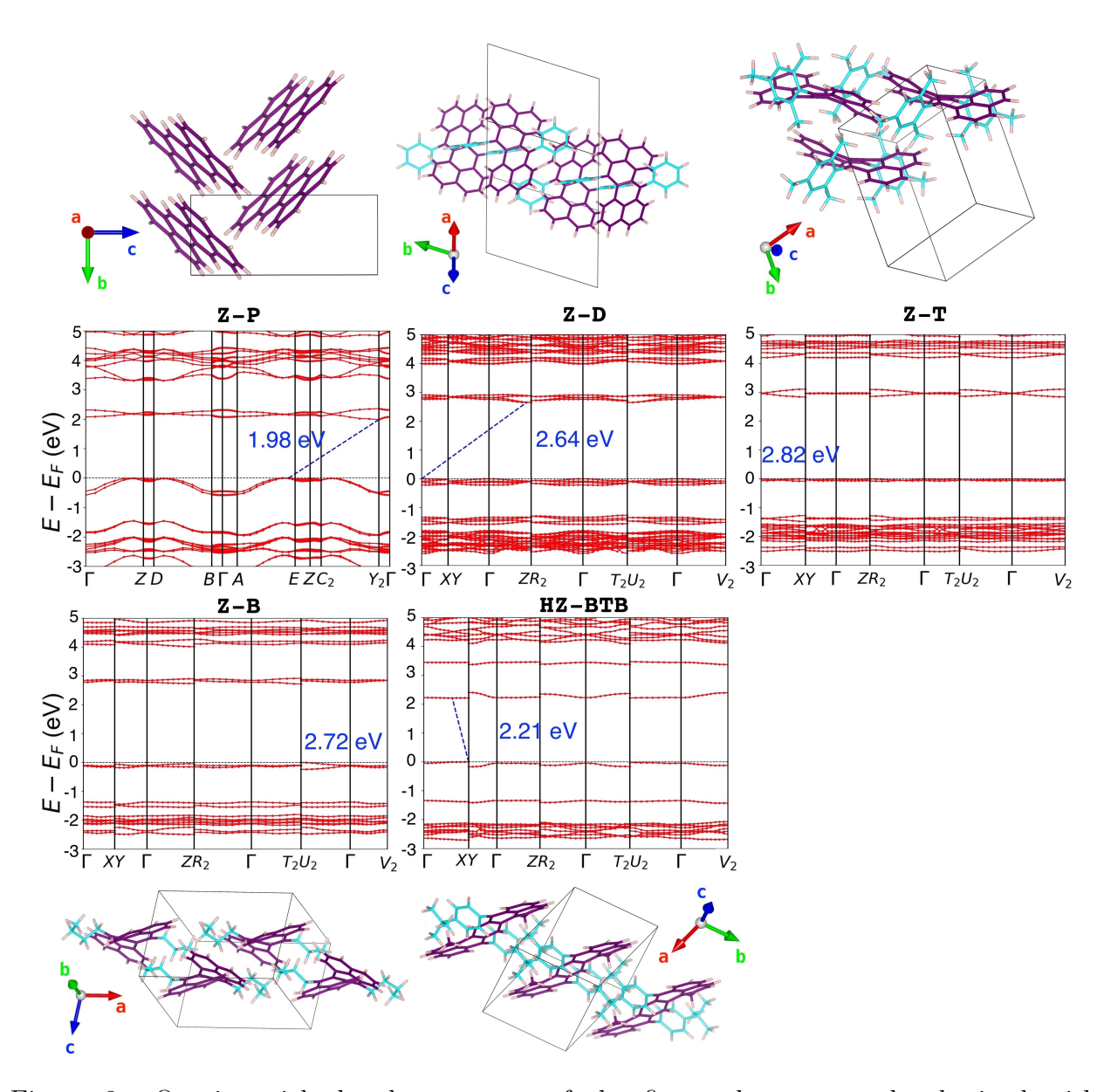


Figure 3: Quasi-particle band structures of the five zethrene crystals obtained with G_0W_0 @PBE. The crystal packing is illustrated next to the corresponding band structures with the backbones and side groups colored in purple and cyan, respectively. The band gap values are shown on each band structure plot.

obtained with G_0W_0 @PBE. Illustrations of the crystal structures are also shown. Of the four zethrenes derivatives, Z-P, which has no side groups, has a herringbone (HB) packing motif, similar to acene crystals. Z-D, Z-T, and Z-B, whose side groups create steric hindrance are slip stacked with larger distances and less cofacial interactions between the zethrene backbones. The different packing motifs lead to different band structures. Z-D, Z-T, and Z-B have approximately the same band gap of around 2.7 eV and relatively flat bands. The stronger cofacial interactions in Z-P, in which the shortest distance between the backbones of neighboring molecules is approximately 3.42Å, leads to a significantly different band structure. Z-P has a smaller band gap of 1.98 eV and more dispersed bands, which may be attributed to the cofacial inter-molecular interactions in the HB structure. The heptazethrene derivative, HZ-BTB, is also slip stacked due to its bulky side groups. Less co-facial interactions leads to relatively flat bands, similar to that of slip-stacked Z-D, Z-T, and Z-B. The band gap of HZ-BTB is 2.21 eV, which is about 0.5 eV smaller than the slip-stacked zethrene derivatives. This may be attributed to the longer backbone, which creates a larger aromatic system and hence smaller energy difference between HOMO and LUMO.

The absorption spectra of the five zethrenes calculated with GW+BSE@PBE are shown in the Figure 4. The absorption spectra of tetracene and pentacene are shown for comparison. Because no experimental data are available for the specific compounds studied here, we compare the optical gap (the lowest singlet exciton energy) to experimental results for similar systems reported in Ref. ⁹³ The computed optical gaps of the Z-D, Z-T, and Z-B crystals are 2.23, 2.37, and 2.35 eV, respectively, slightly higher than the experimentally measured gap of the zethrene derivative in Ref., ⁹³ 2.02 eV, whereas the optical gap of Z-P, 1.86 eV, is slightly lower. The theoretical result for the heptazethrene derivative HZ-BTB, 1.79 eV, is very close to the averaged experimental optical gaps of the heptazethrene derivatives reported in Ref., ⁹³ 1.80 eV. The optical gaps of Z-P and HZ-BTB are comparable to pentacene. However, the main absorption peak of Z-P is centered around 2.5 eV, which is higher than the main absorption peak of pentacene. The main absorption peak of HZ-BTB is in a similar range

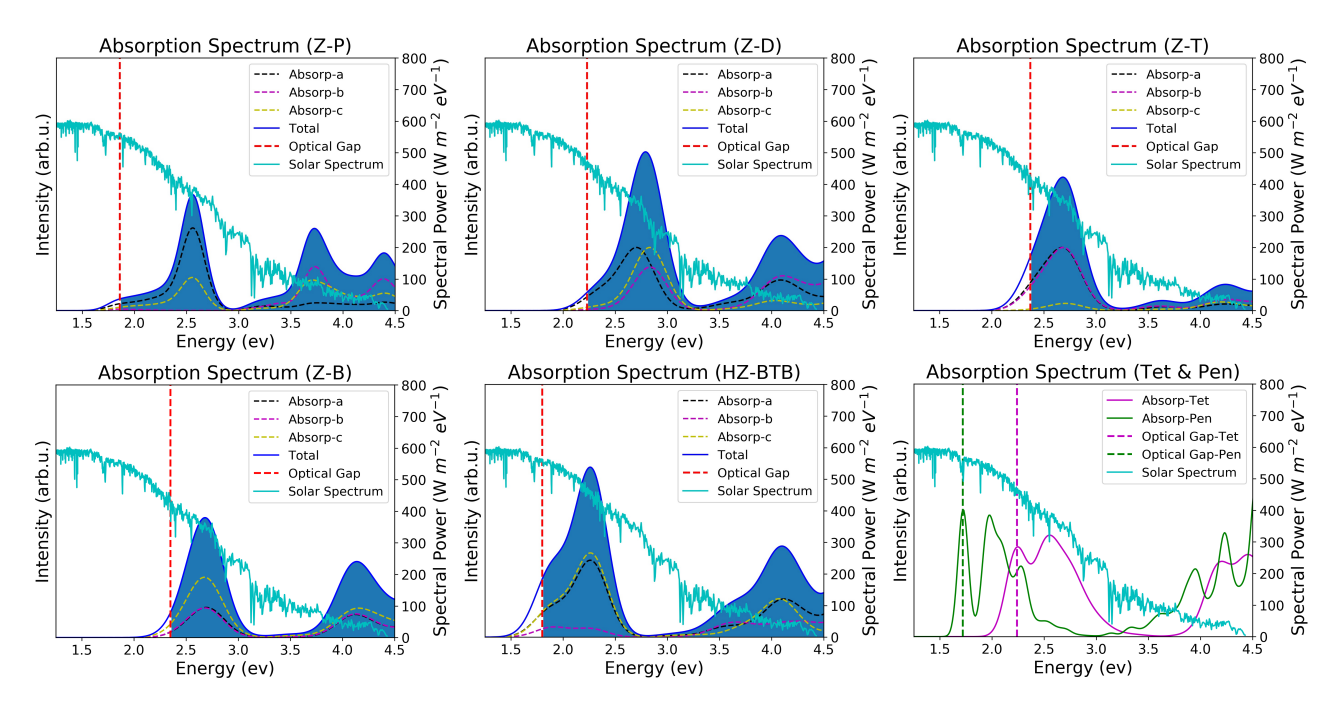


Figure 4: The absorption spectra of Z-P, Z-D, Z-T, Z-B, and HZ-BTB, calculated using GW+BSE@PBE. The absorption spectra for light polarized along the a, b, and c crystal axes are represented by dashed black, magenta, and yellow lines. The total absorption spectra are plotted as solid blue lines. The optical gaps are indicated by red dashed lines. The calculated absorption spectra of tetracene and pentacene are shown for comparison. The solar spectrum 92 is illustrated as a solid cyan line.

to pentacene. The optical gaps of Z-D, Z-T, and Z-B are comparable to tetracene and they absorb in a similar range.

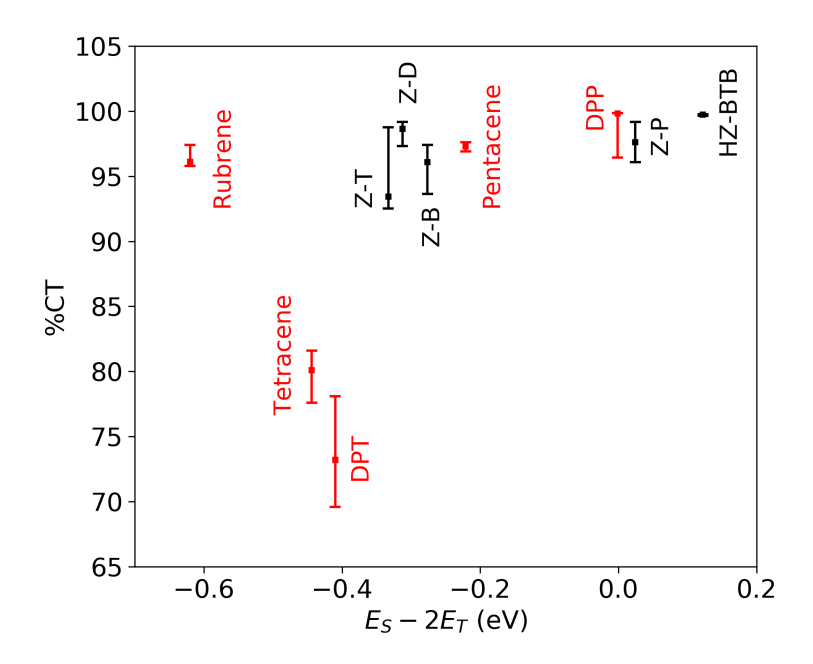


Figure 5: A two-dimensional descriptor for assessing SF candidates. The thermodynamic driving force for SF $(E_{S_1} - 2E_{T_1})$ is plotted on the x-axis and the singlet exciton charge transfer character (%CT) is plotted on the y-axis. The error bars correspond to the range of %CT values obtained using different hole positions when performing double-bader analysis. The results for tetracene, pentacene, rubrene, DPT, and DPP are colored in red to indicate that they have been experimentally observed to undergo SF.

To assess the zethrene derivative as potential SF candidates we employ a two-dimensional descriptor based on the thermodynamic driving force for SF and the degree of singlet exciton charge transfer character. ^{14,15,21} In Figure 5 the SF driving force obtained from GW+BSE@PBE is plotted on the x-axis and the degree of singlet exciton charge transfer character (%CT) obtained from double-Bader analysis is plotted on the y-axis. Tabulated values are provided in the SI. The zethrene crystals are compared to acene derivatives known to exhibit SF in the solid state: tetracene, pentacene, rubrene, diphenyltetracene (DPT), and diphenylpentacene (DPP). ¹⁴ Of the materials studied here, the heptazethrene derivative HZ-BTB exhibits the highest SF driving force, significantly higher than pentacene and DPP, and the highest %CT. This indicates that HZ-BTB could be an outstanding SF candidate. The zethrene derivatives present comparable excitonic properties to the acene derivatives.

The SF driving forces of Z-T, Z-D, and Z-B are about 0.1 eV higher than tetracene and 0.1 eV lower than pentacene. The %CT for these zethrene derivatives is significantly higher than tetracene and DPT and close to pentacene. This means that Z-T, Z-D, and Z-B could potentially undergo SF with a higher triplet yield than tetracene and with fewer losses than pentacene. Z-P is located close to DPP in Figure 5, which implies its SF performance could be similar to that of DPP. It is interesting to note that Z-P has a significantly higher SF driving force than its derivatives Z-T, Z-D, and Z-B. The difference between zethrene and its derivatives is larger than the difference between tetracene and ruberene and the difference between pentacene and DPP. The difference between zethrene and its derivatives may be attributed primarily to their gas-phase excitonic properties. As shown in Figure 2, Z-B, Z-D, and Z-T have a similar SF driving force, which is about 0.4 eV lower than that of Z-P. Moreover, as shown in Figure 3, the steric hindrance caused by the side groups of Z-B, Z-D, and Z-T leads to a different packing arrangement than Z-P and hence to different excitonic properties in the solid state. Thus, functionalizing zethrene with side groups may significantly alter its excitonic properties.

Beyond the degree of singlet exciton CT character, the different packing motifs of the crystals studied here lead to different exciton distributions, which may have implications for the entropic contribution to SF.^{26,45} Both Z-P and HZ-BTB have a higher degree of singlet exciton charge transfer character than tetracene. However, as shown in Figure 6, their exciton wave-functions have different characteristics. Both the Z-P and tetracene crystals have HB packing. In tetracene, the electron probability density is distributed over a shell of neighboring molecules surrounding the molecule on which the hole is located. In contrast, in Z-P the electron charge mainly distributes over the stack of molecules parallel to the molecule on which the hole is located, but barely transfers to adjacent rows. The singlet exciton wavefunctions of the zethrene derivatives Z-B, Z-D, and Z-T display similar characteristics, as shown in the SI. In contrast, in HZ-BTB the electron charge mainly transfers to the two neighboring slipped stacks but barely distributes along the stack parallel to the molecule on

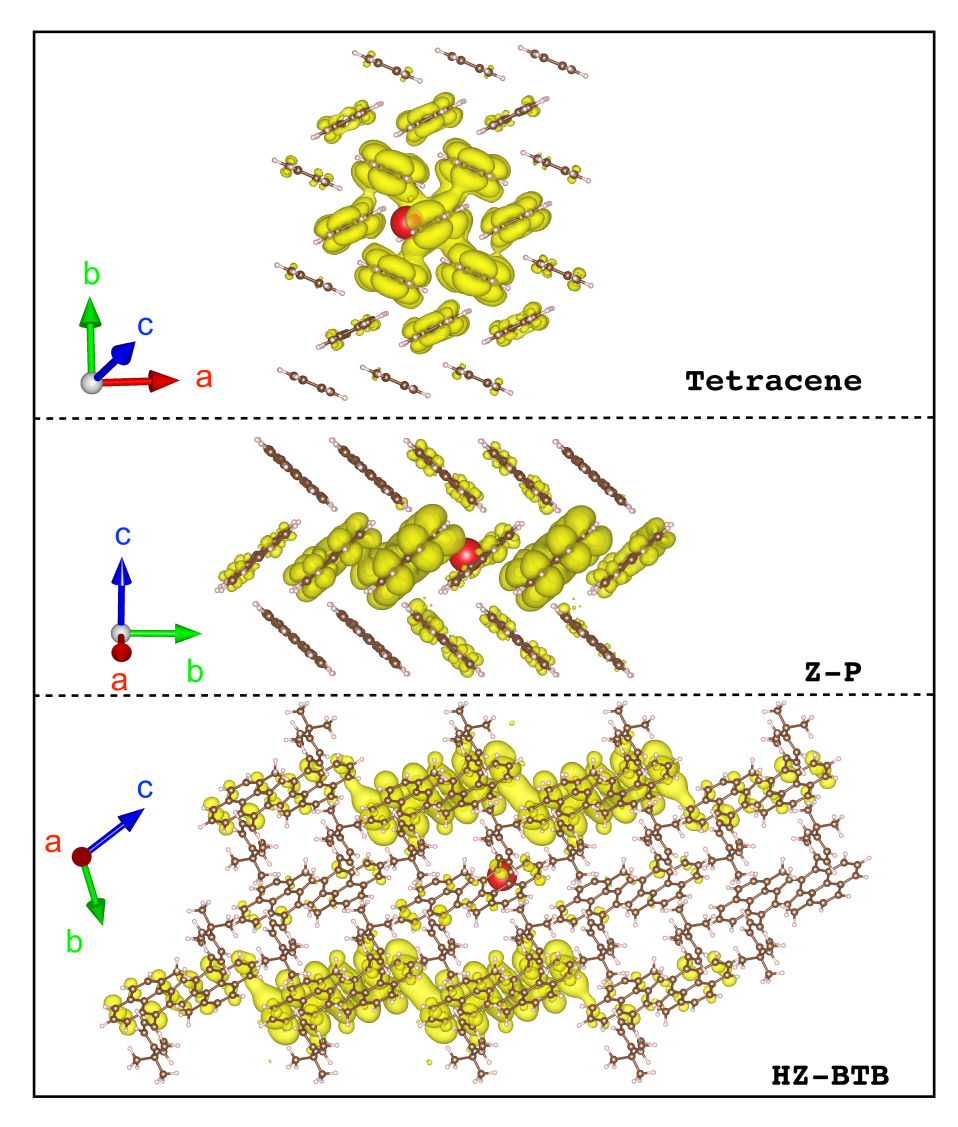


Figure 6: The singlet exciton wave-functions for tetracene, Z-P, and HZ-BTB. The red sphere indicates the hole position and the electron density distribution is shown in yellow.

which the hole resides. This difference may be attributed to the different packing motifs of Z-P and HZ-BTB. In the HB structure of Z-P alternate stacks of parallel molecules have different orientations. In the slip-stacked structure of HZ-BTB all molecules have the same orientation.

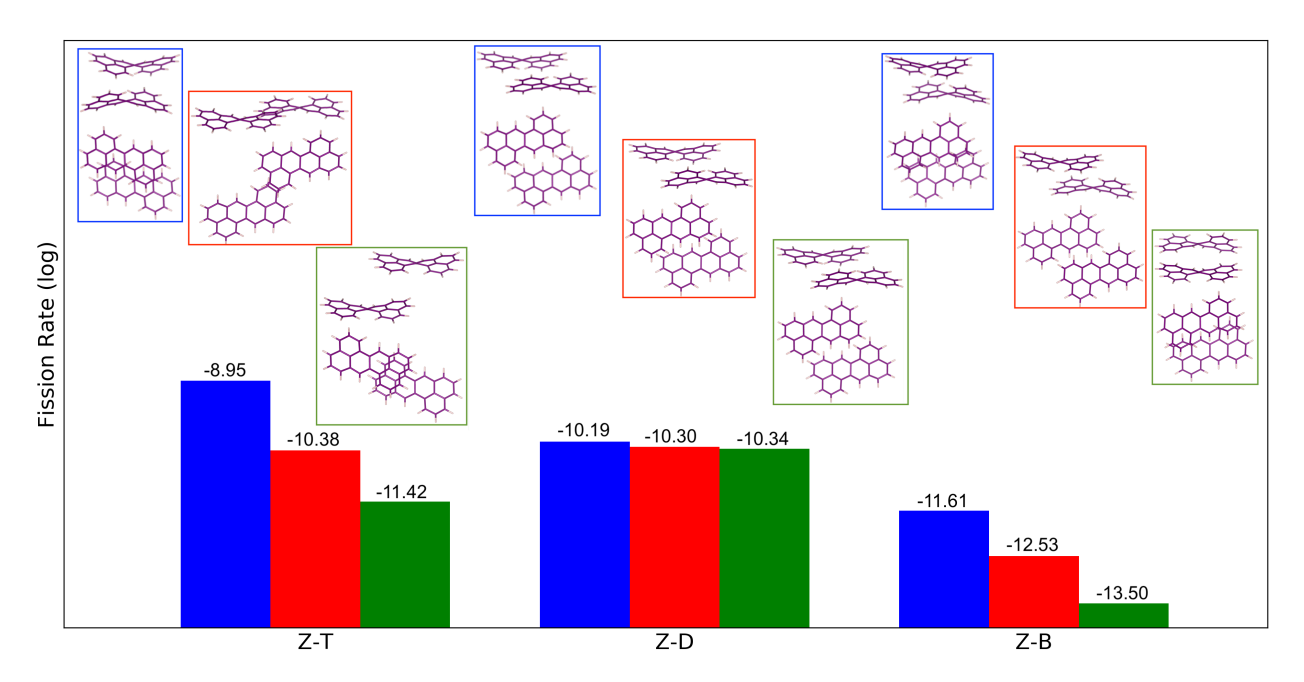


Figure 7: The highest three fission rates for dimers extracted from Z-T, Z-D, and Z-B with side view (top) and top view (bottom) illustrations of the corresponding dimer structures.

Finally, to investigate the effect of crystal packing on SF rates, we use Simple to compare the three zethrene derivatives, Z-T, Z-D, and Z-B, whose different side groups lead to different packing arrangements. Due to the assumptions of the model, Simple can only be used to compare the fission rates among different dimers of the same molecule with the same frontier orbitals. ³² In order to make the three zethrene derivatives comparable, the side groups of Z-T, Z-D, and Z-B were replaced with hydrogen atoms. Z-P was excluded from this comparison because in this structure the zethrene backbone adopts a planar conformation, whereas Z-T, Z-D, and Z-B have a twisted backbone conformation, and the conformational change may affect the frontier orbitals. HZ-BTB is not included because of its larger backbone. We note that the fission rates produced by Simple are approximate and should only be used for qualitative comparisons.

Figure 7 shows the fission rates obtained with Simple for the three best dimers out of each crystal structure with visualizations of their dimer structures. The differences in the crystal packing of Z-T, Z-D, and Z-B lead to changes in orders of magnitude in the predicted fission rates. The highest fission rate of $10^{-8.95}s^{-1}$ is found for a dimer extracted from the Z-T structure. The three dimers extracted from the Z-D crystal structure have intermediate fission rates of the order of $10^{-10}s^{-1}$, similar to the dimer with the second highest rate in Z-T. The dimers extracted from the Z-B crystal structure yield significantly lower rates, the highest of which is $10^{-11.61}s^{-1}$. Of these three materials, whose SF driving force and singlet exciton CT character are similar (see Figure 5), Z-T is likely to be the best candidate for inter-molecular SF in the solid state, based on kinetic considerations.

Conclusion

In summary, We have assessed zethrene (Z-P), three zethrene derivatives (Z-B, Z-D, and Z-T), and a heptazethrene derivative (HZ-BTB) as candidate materials for intermolecular SF in the solid state. These materials were evaluated with respect to multiple descriptors, including the single molecule multi-radical characters, many-body perturbation theory calculations of the thermodynamic driving force for SF and the singlet exciton charge transfer character in crystals, and the Simple kinetic model based on molecular dimers extracted from the crystal structures. In addition, we have compared the zethrenes to acenes known to exhibit SF. All zethrene and heptazethrene derivatives studied here satisfy the SF feasibility condition based on their multi-radical characters. Z-P and HZ-BTB have an exceptionally high SF driving force, compared to pentacene and its derivative DPP, as well as a high singlet exciton charge transfer character. This means that although they are likely to exhibit SF, the energy loss would be considerable. The SF driving force of the zethrene derivatives Z-T, Z-D, and Z-B is higher than tetracene, whose fission process is slightly endoergic, and its derivative DPT, but lower than pentacene. Therefore Z-T, Z-D, and Z-B would be preferable SF materials in

terms of their energy efficiency. The singlet exciton charge transfer character of Z-T, Z-D, and Z-B is higher than tetracene and DPT and close to pentacene. Of these three materials, the Simple kinetic model predicts that the crystal packing of Z-T would yield the fastest SF rate. Therefore, having considered multiple descriptors, Z-T emerges as the most promising SF candidate of the zethrene derivatives studied here. Our approach of considering multiple descriptors may be used by us and others to evaluate additional candidate materials for SF.

Acknowledgement

We thank Prof. Josef Michl, who inspires us with his bold ideas, his resilience, and his great sense of humor. We thank Dr. Eric Anthony Buchanan from University of Colorado Boulder, and Alexandr Zaykov from the Czech Academy of Sciences for help with Simple calculations. We thank Dr. Ryohei Kishi and Dr. Masayoshi Nakano from Osaka University for helpful discussions on calculating the multi-radical characters. Funding was provided by the National Science Foundation (NSF) Division of Materials Research through grant DMR-1844484. This research used resources of the Argonne Leadership Computing Facility (ALCF), which is a DOE Office of Science User Facility supported under contract no. DE-AC02-06CH11357 and of the National Energy Research Scientific Computing Center (NERSC), a DOE Office of Science User Facility supported by the Office of Science of the U.S. Department of Energy under contract no. DE-AC02-05CH11231.

Supporting Information Available

Tabulated multi-radical characters and GW+BSE results; Additional plots of exciton wavefunctions; Superexchange coupling values obtained from Simple for different dimers.

References

- (1) Smith, M. B.; Michl, J. Singlet Fission. Chemical Reviews 2010, 110, 6891–6936.
- (2) Smith, M. B.; Michl, J. Recent Advances in Singlet Fission. *Annual Review of Physical Chemistry* **2013**, *64*, 361–386.
- (3) Monahan, N.; Zhu, X.-Y. Charge Transfer-Mediated Singlet Fission. *Annual Review of Physical Chemistry* **2015**, *66*, 601–618.
- (4) Casanova, D. Theoretical Modeling of Singlet Fission. *Chemical Reviews* **2018**, *118*, 7164–7207.
- (5) Michl, J. Unconventional Solar Energy: Singlet Fission. *Molecular Frontiers Journal* **2019**, 03, 84–91.
- (6) Michl, J. Singlet Fission: Toward More Efficient Solar Cells. Substantia 2019, 45–54.
- (7) Shockley, W.; Queisser, H. J. Detailed balance limit of efficiency of p-n junction solar cells. *Journal of Applied Physics* **1961**, *32*, 510–519.
- (8) Rühle, S. Tabulated values of the Shockley-Queisser limit for single junction solar cells. Solar Energy 2016, 130, 139–147.
- (9) Hanna, M. C.; Nozik, A. J. Solar conversion efficiency of photovoltaic and photoelectrolysis cells with carrier multiplication absorbers. *Journal of Applied Physics* 2006, 100.
- (10) Casillas, R.; Papadopoulos, I.; Ullrich, T.; Thiel, D.; Kunzmann, A.; Guldi, D. M. Molecular insights and concepts to engineer singlet fission energy conversion devices. *Energy Environ. Sci.* 2020, 13, 2741–2804.

- (11) Rao, A.; Wilson, M. W.; Hodgkiss, J. M.; Albert-Seifried, S.; Bässler, H.; Friend, R. H. Exciton fission and charge generation via triplet excitons in pentacene/C60 bilayers.

 *Journal of the American Chemical Society** 2010, 132, 12698–12703.
- (12) Wilson, M. W.; Rao, A.; Johnson, K.; Gélinas, S.; Di Pietro, R.; Clark, J.; Friend, R. H. Temperature-independent singlet exciton fission in tetracene. *Journal of the American Chemical Society* **2013**, *135*, 16680–16688.
- (13) Rao, A.; Friend, R. H. Harnessing singlet exciton fission to break the Shockley-Queisser limit. *Nature Reviews Materials* **2017**, 2, 1–12.
- (14) Wang, X.; Liu, X.; Tom, R.; Cook, C.; Schatschneider, B.; Marom, N. Phenylated Acene Derivatives as Candidates for Intermolecular Singlet Fission. *Journal of Physical Chemistry C* 2019, 123, 5890–5899.
- (15) Liu, X.; Tom, R.; Wang, X.; Cook, C.; Schatschneider, B.; Marom, N. Pyrene-stabilized acenes as intermolecular singlet fission candidates: Importance of exciton wave-function convergence. *Journal of Physics Condensed Matter* **2020**, *32*.
- (16) Ryerson, J. L.; Schrauben, J. N.; Ferguson, A. J.; Sahoo, S. C.; Naumov, P.; Havlas, Z.; Michl, J.; Nozik, A. J.; Johnson, J. C. Two thin film polymorphs of the singlet fission compound 1,3-diphenylisobenzofuran. *Journal of Physical Chemistry C* 2014, 118, 12121–12132.
- (17) Eaton, S. W.; Shoer, L. E.; Karlen, S. D.; Dyar, S. M.; Margulies, E. A.; Veld-kamp, B. S.; Ramanan, C.; Hartzler, D. A.; Savikhin, S.; Marks, T. J., et al. Singlet exciton fission in polycrystalline thin films of a slip-stacked perylenediimide. *Journal of the American Chemical Society* 2013, 135, 14701–14712.
- (18) Eaton, S. W.; Miller, S. A.; Margulies, E. A.; Shoer, L. E.; Schaller, R. D.; Wasielewski, M. R. Singlet exciton fission in thin films of tert -butyl-substituted terrylenes. *Journal of Physical Chemistry A* 2015, 119, 4151–4161.

- (19) Levine, A. M.; Schierl, C.; Basel, B. S.; Ahmed, M.; Camargo, B. A.; Guldi, D. M.; Braunschweig, A. B. Singlet Fission in Combinatorial Diketopyrrolopyrrole-Rylene Supramolecular Films. *Journal of Physical Chemistry C* 2019, 123, 1587–1595.
- (20) Minami, T.; Ito, S.; Nakano, M. Theoretical study of singlet fission in oligorylenes.

 *Journal of Physical Chemistry Letters 2012, 3, 2719–2723.
- (21) Wang, X.; Liu, X.; Cook, C.; Schatschneider, B.; Marom, N. On the possibility of singlet fission in crystalline quaterrylene. *Journal of Chemical Physics* **2018**, *148*.
- (22) Sanders, S. N.; Kumarasamy, E.; Pun, A. B.; Trinh, M. T.; Choi, B.; Xia, J.; Taffet, E. J.; Low, J. Z.; Miller, J. R.; Roy, X., et al. Quantitative Intramolecular Singlet Fission in Bipentacenes. *Journal of the American Chemical Society* 2015, 137, 8965–8972.
- (23) Busby, E.; Xia, J.; Wu, Q.; Low, J. Z.; Song, R.; Miller, J. R.; Zhu, X. Y.; Campos, L. M.; Sfeir, M. Y. A design strategy for intramolecular singlet fission mediated by charge-transfer states in donor-acceptor organic materials. *Nature Materials* **2015**, 14, 426–433.
- (24) Lukman, S.; Chen, K.; Hodgkiss, J. M.; Turban, D. H.; Hine, N. D.; Dong, S.; Wu, J.; Greenham, N. C.; Musser, A. J. Tuning the role of charge-transfer states in intramolecular singlet exciton fission through side-group engineering. *Nature Communications* **2016**, 7, 1–13.
- (25) Broch, K.; Dieterle, J.; Branchi, F.; Hestand, N. J.; Olivier, Y.; Tamura, H.; Cruz, C.; Nichols, V. M.; Hinderhofer, A.; Beljonne, D., et al. Robust singlet fission in pentacene thin films with tuned charge transfer interactions. *Nature Communications* **2018**, *9*.
- (26) Chan, W. L.; Ligges, M.; Zhu, X. Y. The energy barrier in singlet fission can be overcome through coherent coupling and entropic gain. *Nature Chemistry* **2012**, *4*, 840–845.

- (27) Lee, J.; Jadhav, P.; Reusswig, P. D.; Yost, S. R.; Thompson, N. J.; Congreve, D. N.; Hontz, E.; Van Voorhis, T.; Baldo, M. A. Singlet exciton fission photovoltaics. *Accounts of Chemical Research* 2013, 46, 1300–1311.
- (28) Congreve, D. N.; Ji, L.; Thompson, N. J.; Hontz, E.; Yost, S. R.; Reusswig, P. D.; Bahlke, M. E.; Reineke, S.; Van Voorhis, T.; Baldo, M. A. External Quantum efficiency Above 100% in a Singlet-Exciton-Fission-Based Organic Photovoltaic Cell. Science 2013, 340, 334–337.
- (29) Jadhav, P. J.; Mohanty, A.; Sussman, J.; Lee, J.; Baldo, M. A. Singlet exciton fission in nanostructured organic solar cells. *Nano Letters* **2011**, *11*, 1495–1498.
- (30) Schrauben, J. N.; Zhao, Y.; Mercado, C.; Dron, P. I.; Ryerson, J. L.; Michl, J.; Zhu, K.; Johnson, J. C. Photocurrent enhanced by singlet fission in a dye-sensitized solar cell. ACS Applied Materials and Interfaces 2015, 7, 2286–2293.
- (31) Sutton, C.; Tummala, N. R.; Beljonne, D.; Brédas, J. L. Singlet Fission in Rubrene Derivatives: Impact of Molecular Packing. Chemistry of Materials 2017, 29, 2777– 2787.
- (32) Zaykov, A.; Felkel, P.; Buchanan, E. A.; Jovanovic, M.; Havenith, R. W.; Kathir, R. K.; Broer, R.; Havlas, Z.; Michl, J. Singlet Fission Rate: Optimized Packing of a Molecular Pair. Ethylene as a Model. *Journal of the American Chemical Society* 2019, 141, 17729–17743.
- (33) Piland, G. B.; Bardeen, C. J. How Morphology Affects Singlet Fission in Crystalline Tetracene. *Journal of Physical Chemistry Letters* **2015**, *6*, 1841–1846.
- (34) Buchanan, E. A.; Michl, J. *Photochemistry: Volume 47*; The Royal Society of Chemistry, 2020; Vol. 47; pp 498–516.

- (35) Masoomi-Godarzi, S.; Hall, C. R.; Zhang, B.; Gregory, M. A.; White, J. M.; Wong, W. W. H.; Ghiggino, K. P.; Smith, T. A.; Jones, D. J. Competitive Triplet Formation and Recombination in Crystalline Films of Perylenediimide Derivatives: Implications for Singlet Fission. The Journal of Physical Chemistry C 2020, 124, 11574–11585.
- (36) Wang, X.; Garcia, T.; Monaco, S.; Schatschneider, B.; Marom, N. Effect of crystal packing on the excitonic properties of rubrene polymorphs. *CrystEngComm* **2016**, *18*, 7353–7362.
- (37) Arias, D. H.; Ryerson, J. L.; Cook, J. D.; Damrauer, N. H.; Johnson, J. C. Polymorphism influences singlet fission rates in tetracene thin films. *Chemical Science* **2016**, *7*, 1185–1191.
- (38) Chan, W.-L.; Berkelbach, T. C.; Provorse, M. R.; Monahan, N. R.; Tritsch, J. R.; Hybertsen, M. S.; Reichman, D. R.; Gao, J.; Zhu, X.-Y. The Quantum Coherent Mechanism for Singlet Fission: Experiment and Theory. Accounts of Chemical Research 2013, 46, 1321–1329, PMID: 23581494.
- (39) Kim, V. O.; Broch, K.; Belova, V.; Chen, Y. S.; Gerlach, A.; Schreiber, F.; Tamura, H.; Della Valle, R. G.; D'Avino, G.; Salzmann, I.; Beljonne, D.; Rao, A.; Friend, R. Singlet exciton fission via an intermolecular charge transfer state in coevaporated pentacene-perfluoropentacene thin films. *The Journal of Chemical Physics* **2019**, *151*, 164706.
- (40) Miyata, K.; Conrad-Burton, F. S.; Geyer, F. L.; Zhu, X.-Y. Triplet Pair States in Singlet Fission. *Chemical Reviews* **2019**, *119*, 4261–4292.
- (41) Margulies, E. A.; Logsdon, J. L.; Miller, C. E.; Ma, L.; Simonoff, E.; Young, R. M.; Schatz, G. C.; Wasielewski, M. R. Direct Observation of a Charge-Transfer State Preceding High-Yield Singlet Fission in Terrylenediimide Thin Films. *Journal of the American Chemical Society* 2017, 139, 663–671, PMID: 27977196.

- (42) Burdett, J. J.; Bardeen, C. J. Quantum beats in crystalline tetracene delayed fluorescence due to triplet pair coherences produced by direct singlet fission. *Journal of the American Chemical Society* **2012**, *134*, 8597–8607.
- (43) Sharifzadeh, S.; Wong, C. Y.; Wu, H.; Cotts, B. L.; Kronik, L.; Ginsberg, N. S.; Neaton, J. B. Relating the Physical Structure and Optoelectronic Function of Crystalline TIPS-Pentacene. *Advanced Functional Materials* **2015**, *25*, 2038–2046.
- (44) Hart, S. M.; Silva, W. R.; Frontiera, R. R. Femtosecond stimulated Raman evidence for charge-Transfer character in pentacene singlet fission. *Chemical Science* 2018, 9, 1242–1250.
- (45) Kolomeisky, A. B.; Feng, X.; Krylov, A. I. A simple kinetic model for singlet fission: A role of electronic and entropic contributions to macroscopic rates. *Journal of Physical Chemistry C* 2014, 118, 5188–5195.
- (46) Sharifzadeh, S.; Darancet, P.; Kronik, L.; Neaton, J. B. Low-energy charge-transfer excitons in organic solids from first-principles: The case of pentacene. *Journal of Physical Chemistry Letters* 2013, 4, 2197–2201.
- (47) Paci, I.; Johnson, J. C.; Chen, X.; Rana, G.; Popović, D.; David, D. E.; Nozik, A. J.; Ratner, M. A.; Michl, J. Singlet fission for dye-sensitized solar cells: Can a suitable sensitizer be found? *Journal of the American Chemical Society* 2006, 128, 16546– 16553.
- (48) Minami, T.; Nakano, M. Diradical character view of singlet fission. *Journal of Physical Chemistry Letters* **2012**, *3*, 145–150.
- (49) Nakano, M. Open-Shell-Character-Based Molecular Design Principles: Applications to Nonlinear Optics and Singlet Fission. *Chemical Record* **2017**, *17*, 27–62.

- (50) Ito, S.; Minami, T.; Nakano, M. Diradical Character Based Design for Singlet Fission of Condensed-Ring Systems with 4n Electrons. The Journal of Physical Chemistry C 2012, 116, 19729–19736.
- (51) Lo, D.; Ruipe, F. Theoretical design of conjugated diradicaloids as singlet fission sensitizers: quinones and methylene derivatives †. **2017**, 6, 30227–30238.
- (52) Ito, S.; Nagami, T.; Nakano, M. Molecular design for efficient singlet fission. *Journal of Photochemistry and Photobiology C: Photochemistry Reviews* **2018**, *34*, 85 120.
- (53) Alagna, N.; Han, J.; Wollscheid, N.; Lustres, J. L. P.; Herz, J.; Hahn, S.; Koser, S.; Paulus, F.; Bunz, U. H.; Dreuw, A., et al. Tailoring Ultrafast Singlet Fission by the Chemical Modification of Phenazinothiadiazoles. *Journal of the American Chemical* Society 2019, 141, 8834–8845.
- (54) Pensack, R. D.; Tilley, A. J.; Parkin, S. R.; Lee, T. S.; Payne, M. M.; Gao, D.; Jahnke, A. A.; Oblinsky, D. G.; Li, P. F.; Anthony, J. E., et al. Exciton delocalization drives rapid singlet fission in nanoparticles of acene derivatives. *Journal of the American Chemical Society* 2015, 137, 6790–6803.
- (55) Shushin, A. I. Kinetics of singlet fission in organic semiconductors: Specific features of T-exciton migration effects. *Journal of Chemical Physics* **2019**, *151*.
- (56) Yost, S. R.; Lee, J.; Wilson, M. W.; Wu, T.; McMahon, D. P.; Parkhurst, R. R.; Thompson, N. J.; Congreve, D. N.; Rao, A.; Johnson, K., et al. A transferable model for singlet-fission kinetics. *Nature Chemistry* 2014, 6, 492–497.
- (57) Jortner, J.; Bixon, M. Intramolecular vibrational excitations accompanying solvent-controlled electron transfer reactions. *The Journal of chemical physics* **1988**, *88*, 167–170.

- (58) Wu, Q.; Cheng, C.-L.; Van Voorhis, T. Configuration interaction based on constrained density functional theory: A multireference method. The Journal of chemical physics 2007, 127, 164119.
- (59) Van Kampen, N. G. Stochastic processes in physics and chemistry; Elsevier, 1992; Vol. 1.
- (60) Havlas, Z.; Michl, J. Guidance for mutual disposition of chromophores for singlet fission.

 Israel Journal of Chemistry 2016, 56, 96–106.
- (61) Smith, M. B.; Michl, J. Recent advances in singlet fission. *Annual review of physical chemistry* **2013**, *64*, 361–386.
- (62) Havenith, R. W.; de Gier, H. D.; Broer, R. Explorative computational study of the singlet fission process. *Molecular Physics* **2012**, *110*, 2445–2454.
- (63) Berkelbach, T. C.; Hybertsen, M. S.; Reichman, D. R. Microscopic theory of singlet exciton fission. I. General formulation. The Journal of chemical physics 2013, 138, 114102.
- (64) Smith, M. B.; Michl, J. Singlet fission. Chemical Reviews 2010, 110, 6891–6936.
- (65) Hu, P.; Wu, J. Modern zethrene chemistry. Canadian Journal of Chemistry 2017, 95, 223–233.
- (66) Li, Y.; Heng, W. K.; Lee, B. S.; Aratani, N.; Zafra, J. L.; Bao, N.; Lee, R.; Sung, Y. M.; Sun, Z.; Huang, K. W., et al. Kinetically blocked stable heptazethrene and octazethrene: Closed-shell or open-shell in the ground state? *Journal of the American Chemical Society* 2012, 134, 14913–14922.
- (67) Hsieh, Y. C.; Fang, H. Y.; Chen, Y. T.; Yang, R.; Yang, C. I.; Chou, P. T.; Kuo, M. Y.; Wu, Y. T. Zethrene and dibenzozethrene: Masked biradical molecules. *Angewandte Chemie - International Edition* 2015, 54, 3069–3073.

- (68) Wu, T. C.; Chen, C. H.; Hibi, D.; Shimizu, A.; Tobe, Y.; Wu, Y. T. Synthesis, structure, and photophysical properties of dibenzo-[de, mn]naphthacenes. *Angewandte Chemie International Edition* **2010**, *49*, 7059–7062.
- (69) Kamata, S.; Sato, S.; Wu, J.; Isobe, H. Crystal structure of 7,15-bis(4-tert-butylphenyl)-1,9-dimethylheptazethrene. *Acta Crystallographica Section E: Crystallographic Communications* **2017**, *73*, 99–102.
- (70) Blum, V.; Gehrke, R.; Hanke, F.; Havu, P.; Havu, V.; Ren, X.; Reuter, K.; Scheffler, M. Ab initio molecular simulations with numeric atom-centered orbitals. Computer Physics Communications 2009, 180, 2175–2196.
- (71) Perdew, J. P.; Burke, K.; Ernzerhof, M. Generalized gradient approximation made simple. *Physical Review Letters* **1996**, *77*, 3865–3868.
- (72) Tkatchenko, A.; Scheffler, M. Accurate molecular van der Waals interactions from ground-state electron density and free-atom reference data. *Physical Review Letters* **2009**, *102*, 6–9.
- (73) Marom, N. Accurate description of the electronic structure of organic semiconductors by GW methods. *Journal of Physics Condensed Matter* **2017**, *29*.
- (74) Sharifzadeh, S. Many-body perturbation theory for understanding optical excitations in organic molecules and solids. *Journal of Physics Condensed Matter* **2018**, *30*.
- (75) Golze, D.; Dvorak, M.; Rinke, P. The GW Compendium: A Practical Guide to Theoretical Photoemission Spectroscopy. *Frontiers in Chemistry* **2019**, 7.
- (76) Liu, C.; Kloppenburg, J.; Yao, Y.; Ren, X.; Appel, H.; Kanai, Y.; Blum, V. Allelectron ab initio Bethe-Salpeter equation approach to neutral excitations in molecules with numeric atom-centered orbitals. *Journal of Chemical Physics* **2020**, *152*.

- (77) Ren, X.; Rinke, P.; Blum, V.; Wieferink, J.; Tkatchenko, A.; Sanfilippo, A.; Reuter, K.; Scheffler, M. Resolution-of-identity approach to Hartree-Fock, hybrid density functionals, RPA, MP2 and GW with numeric atom-centered orbital basis functions. New Journal of Physics 2012, 14.
- (78) Jacquemin, D.; Duchemin, I.; Blase, X. Benchmarking the Bethe-Salpeter Formalism on a Standard Organic Molecular Set. *Journal of Chemical Theory and Computation* **2015**, *11*, 3290–3304.
- (79) Deslippe, J.; Samsonidze, G.; Strubbe, D. A.; Jain, M.; Cohen, M. L.; Louie, S. G. BerkeleyGW: A massively parallel computer package for the calculation of the quasi-particle and optical properties of materials and nanostructures. *Computer Physics Communications* **2012**, *183*, 1269–1289.
- (80) Giannozzi, P. et al. QUANTUM ESPRESSO: A modular and open-source software project for quantum simulations of materials. *Journal of Physics Condensed Matter* **2009**, 21.
- (81) Troullier, N.; Martins, J. L. Efficient pseudopotentials for plane-wave calculations. *Physical Review B* **1991**, *43*, 1993–2006.
- (82) Deslippe, J.; Samsonidze, G.; Jain, M.; Cohen, M. L.; Louie, S. G. Coulomb-hole summations and energies for GW calculations with limited number of empty orbitals: A modified static remainder approach. *Physical Review B - Condensed Matter and Materials Physics* 2013, 87, 1–6.
- (83) Knight, J. W.; Wang, X.; Gallandi, L.; Dolgounitcheva, O.; Ren, X.; Ortiz, J. V.; Rinke, P.; Körzdörfer, T.; Marom, N. Accurate Ionization Potentials and Electron Affinities of Acceptor Molecules III: A Benchmark of GW Methods. *Journal of Chemical Theory and Computation* 2016, 12, 615–626.

- (84) Jacquemin, D.; Duchemin, I.; Blondel, A.; Blase, X. Benchmark of Bethe-Salpeter for Triplet Excited-States. Journal of Chemical Theory and Computation 2017, 13, 767– 783.
- (85) Wang, X.; Tom, R.; Liu, X.; Congreve, D. N.; Marom, N. An energetics perspective on why there are so few triplet–triplet annihilation emitters. *Journal of Materials Chemistry C* **2020**, 1.
- (86) Schmidt, M. W.; Baldridge, K. K.; Boatz, J. A.; Elbert, S. T.; Gordon, M. S.; Jensen, J. H.; Koseki, S.; Matsunaga, N.; Nguyen, K. A.; Su, S., et al. General atomic and molecular electronic structure system. *Journal of Computational Chemistry* 1993, 14, 1347–1363.
- (87) Nakano, M.; Fukui, H.; Minami, T.; Yoneda, K.; Shigeta, Y.; Kishi, R.; Champagne, B.; Botek, E.; Kubo, T.; Ohta, K., et al. (Hyper)polarizability density analysis for openshell molecular systems based on natural orbitals and occupation numbers. *Theoretical Chemistry Accounts* **2011**, *130*, 711–724.
- (88) Frisch, M. J.; Trucks, G. W.; Schlegel, H. B.; Scuseria, G. E.; Robb, M. A.; Cheeseman, J. R.; Scalmani, G.; Barone, V.; Petersson, G. A.; Nakatsuji, H., et al. Gaussian 16 Revision C.01. 2016; Gaussian Inc. Wallingford CT.
- (89) Becke, A. D. Becke's three parameter hybrid method using the LYP correlation functional. *J. Chem. Phys* **1993**, *98*, 5648–5652.
- (90) Stephens, P. J.; Devlin, F. J.; Chabalowski, C. F.; Frisch, M. J. Ab initio calculation of vibrational absorption and circular dichroism spectra using density functional force fields. *The Journal of physical chemistry* **1994**, *98*, 11623–11627.
- (91) Naskar, S.; Das, M. The use of low-lying excited states of zethrene and its homologs in singlet fission within Pariser-Parr-Pople model Hamiltonian: A Density Matrix Renormalization Group study. Chemical Physics 2020, 533, 110717.

- (92) Gueymard, C. A. Parameterized transmittance model for direct beam and circumsolar spectral irradiance. *Solar Energy* **2001**, *71*, 325–346.
- (93) Lukman, S.; Richter, J. M.; Yang, L.; Hu, P.; Wu, J.; Greenham, N. C.; Musser, A. J. Efficient Singlet Fission and Triplet-Pair Emission in a Family of Zethrene Diradicaloids. *Journal of the American Chemical Society* 2017, 139, 18376–18385.